EFDA–JET–CP(12)02/16

C.C. Klepper, P. Jacquet, V. Bobkov, L. Colas, T.M. Biewer, D. Borodin, A. Czarnecka, C. Giroud, E. Lerche, V. Martin, M.-L. Mayoral, F. Rimini, G. Sergienko, D. Van Eester and JET EFDA contributors

RF Sheath-Enhanced Beryllium Sources at JET's ICRH Antennas

RF Sheath-Enhanced Beryllium Sources at JET's ICRH Antennas

C.C. Klepper[1], P. Jacquet[2], V. Bobkov[3], L. Colas[4], T.M. Biewer[1], D. Borodin[5], A. Czarnecka[6], C. Giroudx[2], E. Lerche[7], V. Martin[4], M.-L. Mayoral[2], F. Rimini[2], G. Sergienko[5], D. Van Eester[7] and JET EFDA contributors*

JET-EFDA, Culham Science Centre, OX14 3DB, Abingdon, UK

[1]Oak Ridge National Laboratory, Oak Ridge, TN 37831-6169, USA
[2]EURATOM-CCFE Fusion Association, Culham Science Centre, OX14 3DB, Abingdon, OXON, UK
[3]Max-Planck-Institut für Plasmaphysik, EURATOM-Assoziation, Garching, Germany
[4]CEA, IRFM, F-13108 Saint Paul-Lez-Durance, France
[5]Association EURATOM-FZJ, Trilateral Euregio Cluster, 52425 Jülich, Germany
[6]Association Euratom-IPPLM, Hery 23, 01-497 Warsaw, Poland
[7]Association EURATOM-Belgian State, Koninklijke Militaire School-Ecole Royale Militaire, B-1000 Brussels Belgium
** See annex of F. Romanelli et al, "Overview of JET Results", (23rd IAEA Fusion Energy Conference, Daejon, Republic of Korea (2010)).*

Preprint of Paper to be submitted for publication in Proceedings of the
20th International Conference on Plasma Surface Interactions , Eurogress, Aachen, Germany
21st May 2012 - 25th May 2012

ABSTRACT

Local Beryllium (Be) I and Be II line intensities were measured in the plasma-wall interaction region near an ICRH antenna in JET. The intent was to use these intensities as a measure of the formation of local Radio Frequency (RF) sheath potentials, through RF sheath rectification and potential build up at the end of field lines passing in front of the antenna. Experimetally, it was found that the Be I and Be II emission increase when using the antenna local to the spectroscopic measurement, and increase even more when using a remote antenna that is magnetically connected to the observation point. Magnetic field mapping indicates a magnetic connection between the observation location and the top corner region of the remote antenna and/or its protection limiter. These measurements can be used in support of RF sheath modeling that is an important part of the optimization of antenna design for next generation fusion energy devices, including ITER.

1. INTRODUCTION

A topic area of plasma surface interactions of increasing interest pertains to the interaction of the Ion Cyclotron Resonance Heating (ICRH), waves with the Scrape-off layer (SOL) plasma in the vicinity of the launch antenna. In particular, the RF electric field parallel to the (static) magnetic field, $E_{||}$, gives rise to RF sheath potentials [1] in which ions can be accelerated producing problematic localized heating (hot spots) [2], as well as sputtering of and metallic Plasma Facing Components (PFCs) [3, 4]. As such, the formation of such RF sheath potentials is one of the most important factors that can limit operation of ICRH for long-pulse, high-power operation.

While a direct measurement of such RF sheath potentials would be ideal, indirect wayshave been so far more tangible in the large fusion experiment environment. One approach developed on Tore Supra [5, 6] and more recently applied on ASDEX-U, has been to use a reciprocating Langmuir probe magnetically connected to an antenna structure and to measure the plasma potential, while moving the probe to get a radial dependence. Then, the electric field can be computed from the gradient potential. At the same time, sweeping the edge safety factor (qedge) the poloidal variation of the sheath potential can be estimated. The enhanced tungsten (W) sputtering during ICRH in ASDEX Upgrade led to further RF sheath characterisation [3]. Since W production is primarily through physical sputtering, the W flux and the resulting W I emission allow a detection of relative changes in local potentials, as sensitive to the local ion energies, which in turn are sensitive to the RF sheath potentials.

The latter is the approach used recently on JET, in a series of experiments performed with the new ITER-Like Wall (ILW), which consists of mainly beryllium (Be) on the main chamber and tungsten (W) in the divertor. This provided the opportunity to study Be sources from newly installed Be poloidal limiter and from the ICRH antennas which have Be screen bars and following the change of wall, Be private poloidal limiters (referred as antenna septa), and to potentially observe an enhancement of the Be sputtering due to RF-sheaths (as observed with W in ASDEX-Upgrade). The spectroscopic views that were deployed for this study were the ones from the Charge-eXchange

Recombination Spectroscopy (CXRS) diagnostic on JET that terminate on ICRH antenna structures and connected to a spectrometer that allowed access to both Be I and Be II lines. The fact that the CXRS diagnostic is absolute intensity calibrated, should allow for use of the herein presented data for Be erosion studies in conjuction with relevant erosion/redeposition codes. However, in this first paper, the analysis is limited to the use of the spectroscopic signals to indentify regions of enhanced sputtering due to rectified potential around the ICRH antennas. The localization of the measurements is qualitatively confirmed with processed images from visible-range video cameras that view the same antenna and limiter structures.

This paper is organized as follows: In Section II we describe the experimental apparatus and the JET experimental conditions involved in these studies. In Section III we examine how the spectroscopic data correlate with magnetic field line tracing that maps regions of the active antenna onto the observation region on a PFC. In Section IV, we present our conclusions, remaining questions and plans for continued studies and analyses.

2. EXPERIMENTAL ARRANGMENT AND OBSERVATIONS

JET has presently four "traditional" ICRH antennas referred as A, B, C and D and toroidally spaced around the tokamak at $\pi/6$ (between octant 1 and 2), $3\pi/6$ (between octant 2 and 3), $7\pi/6$ (between octant 5 and 6), $8\pi/6$ (between octant 6 and 7) respectively [7], and one "ITER-like" ICRH antenna, not presently in operation. Each of the traditional antennas features four, independenty controlled current straps. In this paper, the Poloidal Limiter (PL) on the left of antenna D, as viewed from the plasma, will be referred to as D-left; similarly Cright will be the PL to the right of ant-C and so forth.

Figure 1 illustrates the geometry of the spectroscopic sightlines involved in this study. Two of the sightlines of the CXRS collection optics at octant 1 and are normally designed to intercept the neutral beams injected from octant 8 at various radial locations. The innermost sightline (labeled '1') falls right on the Faraday screen of the 4^{th} strap of antenna D (4^{th} one on the left viewing from the plasma), referred to as the D4 strap, while the next chord (labeled '2') falls on PL D-left. The tangential nature of these sightlines results in chord '1' passing within 16 cm of the antenna-facing side of PL D-left, while chord '2' would sample more of the region facing away from the antenna. It is reasonable to suppose that the "D4-chord" mostly samples Be emission from the antenna side of the D-left PL. This is consistent with the close distance of this tangential chord to the antenna-facing side of the PL.

Use of the existing CXRS system provided for this study a high-resolusion spectrometer to analyze the collected emission from these antenna structures. The spectral lines of choice were Be I 4572Å (Singlet, 2s3d 1D $\rightarrow$ 2s2p 1P) and Be II 4673Å (4f 2F $\rightarrow$ 3d 2D). These spectral lines were chosen, because they are suitable for future simulation with the ERO code to quantify antenna Be erosion [8]. Since the present detection hardware does not yet allow simultaneous detection of these two spectral lines, the emission from each of these lines was detected in similar shots. The C III 4650 Å was simultaneously detected, in both cases, and used to provide local density normalization.

Since the observed plasmasurface interactions occur on a pure Be surface, the C III line intensity represents local atomic line excitation, but not a local source.

These studies were performed in L-mode plasmas. This has the advantage of quiescent SOL plasma conditions, in which it is possible to resolve small changes on PFCs and the SOL, as a result of changes in the antenna power and/or configuration. The main approach in these studies was to modulate all the available antennas, interweaving these modulations so as to distinguish effect from each antenna. At the same time, plasma edge conditions could be gradually changed to observe changes in each modulation cycle. For these experiments, all 4 straps of antennas C and D were functioning and each of these antennas was operated indepently. Only half (2 straps) of antennas A and B were used. These two antennas were operated at the same time, as A and B are supplied by the same RF generator.

In the top graph of Fig. 2, the ratio of Be I/C III is shown for a JET pulse featuring such an antenna modulation scheme. In this shot (JET Pulse 81173), all available antennas, i.e. C and D, independently (each with all four straps) and A + B jointly (two straps from each), were operated with "-90o phasing" (i.e. current on the straps 90o apart: 135o 45o -45o -135o) and modulated sequencially, as shown in bottom graph of Fig. 2. Superimposed on this graph, the edge q factor is shown decreasing monotonically. This was achieved by sweeping the plasma current at constant toroidal magnetic field Bt, while the outer gap was kept nearly constant. In this particular pulse, the spectrometer was set to the Be I line, off-set enough to also include the C III line within the range of the CCD array of the spectrometer detection camera. For a similar shot (JET Pulse 81172, not shown) the spectrometer was set to Be II. (Be I)/(C III) traces are shown not only for the two mentioned sightlines, but also for a third sightline from the same fan of the CXRS system, which is further out (larger tangency radius) that Chords '1' and '2' and chosen such that its clearly outside the interaction region of the SOL plasma with the antenna and its limiter. This "Outside Chord" then provides a reference or Be emission in the SOL near, but not at any antenna-plasma interaction region.

It is clear from Fig. 2 that both the magnitude of the normalized Be emission and its variation during antenna modulation and q-sweeping are much larger for the chord '1' which passes on the antenna side of PL D-left. This is a first clear indication that the measurement represents a localized Be source, which is related to the operation of the ICRH antennas.

To get a clear view of the dependence of this Be source each of the antennas, the average value of the ratio (Be I or Be II emission)/(C III emission) is evaluated at each antenna plateau and for each cycle, including the no-antenna (OH) gaps in each cycle. The result is shown for the same JET pulse in Fig. 3. Here it is seen that the effect of the C antenna is very different than that of the A&B antenna. What is also remarkable is that this effect of enhanced Be emission (and its strong q-dependence) is substantially stronger with the operation of the remote antenna C than it is with antenna D, even though the observations are made at this antenna and its nearest poloidal limiter. In the next section, a preliminary model of the C-antenna effect will be developed.

Other observations in these experiments were as follows: (1) Pulse 81172, which was identical to 81173 except that the spectrometer was set to the Be II/C III set of lines, shows nearly the same dependence for this ratio as the Be I/C III ratio in 81173. This indicates that Be I and Be II are similarly localized and it suffices to measure one of these to study Be production at the PL. (2) From the raw (un-normalized) signals it was found that the sharp increases in either Be I/C III or Be II/C III was predominantly due to the Be lines and not the C III. (3) The increase in the Be source when antenna C is active was also found to be strongly dependent on the antenna phasing. In the above mentioned JET pulses, all the antennas were operated in –90o phasing. In JET ICRH pulses, carried out under similar discharge and antenna timing conditions, but with the antennas configured with a dipole phasing (i.e. current on the straps 180o apart: -90o 90o -90o 90o), the enhancement in apparent Be production is 2-3 times lower that with -90o phasing. A similar impact of antenna phasing can be seen in the enhanced release of Ni [9] and W [4] when using ICRH heating.

3. INTERPRETATION

Further analysis of Pulse No's: 81172/81173 shows clear differences in both the sensitivity and the q_{95} dependence of the emission from the antenna-side of the D-left limiter on which antenna is active. This is seen in Fig. 3, where the averages over each antenna plateau and over each cycle of the modulation sequence are plotted versus q_{95} and sorted by antenna. In particular, it is noticed that the C-antenna effect is high on both sides of the q-scan. It is also clear again that the Be source is higher with antenna C than with any other antenna, over the whole range of the q-scan.

A clear link between the observation region at the midplace position of the D-left poloidal limiter and the top of Antenna C is obtained with EFIT-aided, magnetic field line tracing shown in Fig.4. This suggests that the enhanced local Be source when using antenna C could be related to the higher $E_{||}$ values at the top and bottom of antenna structures, predicted by antenna models [10]. However, further work is needed to compare JET antenna calculated $E_{||}$ spatial maps and expected RF rectified potentials at limiter's surface to our experimental observations.

It is worth noting that there is an alternative interpretation for the appearance of a minimum in the C-ant curve of Fig.3, other that as a transition between magnetic connection between the two ant-C corners: The tilt of the Faraday screen rods is intended to eliminate the slow wave field component of the excited electric field and hence to minimize the acceleration of particles along the magnetic field lines in the edge region. The q-scan alters the relative pitch of the Faraday screen bars and Bt.

It is also seen in Fig.3 that, with the combined A&B-antennas, the Be source increases monotonically with q_{95}. When looking at only the Ohmic Heating (OH) data, the effect also increases monotonically with q_{95} but not at same rate as A&B effect. Nevertheless it is possible that both the ohmic and the A&B-antenna effects could be attributed to a background (non-local) Be emission, not corrected by the division of the Be I and II lines by the C III line. The fact that the spectroscopy observation point gets magnetically connected to a poloidal limiter close to antennas A&B when q_{95} increase could also provide an explanation for the increase in Be signal when A&B were energized.

One way to investigate these effects, overcoming the spatial limitation of the sightlinebased spectroscopic study, is to use cameras that spatially image the emission at the PLs. Unfortunately, for these early JET ILW ICRH studies, the only camera images obtained with Be line-filtered cameras (Be II 527nm) viewed other PLs than the one accessed with the spectrometer. Furthermore, the sensitivity at the antenna limiters was too low during diverted discharges to draw useful conclusions. However, a dual color camera set (referred as KL12) collected images from the same region as the spectrometer and with a similar tangential view. The top of Fig.5 shows a processed image from this camera for the same shot as in Figures 2 and 3, at $q_{95} = 3$. (The processing involves time averaging compatible with the modulation experiment and background taken from a region of the image not exhibiting antennadependent features). This image is actually produced with two mirrors that the KL12 camera uses to access the full vertical extend of the plasma. The two peaks seen around the midplane section of the PL are in fact the same peak and the apparent split is an artifact of the merging of the two images. Although it is not clear what line emission dominates in the formation of this peak feature, it is consistent with the timing of the appearance of the maximum emission in the spectroscopic measurement when antenna C is on.

The q-dependence is shown more explicitly in the bottom of Fig.5. Here this is done by averaging over "Regions Of Interest" (ROIs) equally dividing the luminous poloidal extent of the PL. The spatially averaged intensity from each ROI is then time-averaged over each antenna C plateau, and from this the time-average over the corresponding antenna A&B plateau was subtracted. Due to the mentioned imaging artifact, ROIs -12 and -15 correspond to the same physical region, which is also the poloidal location of the spectroscopic measurement. It is seen that q-dependence of the emission in this region is quite similar to the low-q side of the q-dependence of the C-antenna curve of Fig.3. However, the rise with q on the high-q side is not seen. This q-dependence is qualitatively similar to what one also would get in the spectroscopic data of Fig.3, if either the ohmic or the A&B curve was used as the background for the C-ant data. When the same image analysis is performed for the times with the D-ant active, a bright spot is found much higher on the same PL and thus outside the view of the spectroscopic sightlines. Although this study would be worth repeating with a Be-line-filtered camera, this color image analysis confirms the presence of a significant change is plasma emission with the same q95 and at the same location as the spectroscopic measurement.

CONCLUSIONS AND NEXT STEPS

The results presented herein indicate a clear correlation between localized, enhanced Be line emission at poloidal limiters and possible effect of inhomogenous RF-sheath potential on or around active antennas. This constitutes a direct, experimental confirmation of rf rectified sheath potentials on PFCs magnetically connected to energized antennas. Since present ICRH antennas models predict such effect, this study is also an important step toward experimental verification of ICRH antenna and RF-sheath models.

The next logical step would be to connect these results with RF-sheath modeling specific to the

JET A2 antennas, which is on-going [4]. The main interest would be to confirm the appearance of higher sheath potential regions at the top (and bottom) corners of the antenna and/or its protective PLs, as suggested by the stronger effect of the C-ant, than that of the D-ant, on the Be produced at PL D-left. In addition, modeling would be helpful to understand the physics involved in the phasing-dependence of enhanced Be production, as well any potentially "global" effects from the joint operation of antennas A and B, to explain the stronger dependence of the A&B-ant induced emission at the D-left PL.

Other plans include (1) the improvement of camera imaging of ICRH antenna and protection limiters to get useful Be I or Be II line-filtered data, (2) connection of the measurements to ADAS atomic physics models and to Be erosion models (such as currently evolving versions of the ERO code [8]) – folding in the actual geometry of the sightlines - to get a preliminary evaluation of Be erosion in L-mode discharges, and (3) extension of these studies to H-mode. The latter is possible, since Be II line monitoring is compatible with CXRS on the Be IV CX line which can be simultaneously measured.

ACKNOWLEDGEMENT

This work was supported by the US DOE under Contract No. DE-AC05-00OR22725 with UT-Battelle, LLC. This work was also supported by EURATOM and carried out within the framework of the European Fusion Development Agreement. The views and opinions expressed herein do not necessarily reflect those of the European Commission.

REFERENCES

[1]. D.A. D'Ippolito and J.R. Myra, Journal of Nuclear Materials **415** (2011) S100
[2]. Ph. Jacquet, this proeedings [this conference, Poster P1-20]
[3]. V. Bobkov et al., Nuclear Fusion **50** (2010) 035004
[4]. V. Bobkov, these proceedings
[5]. L. Colas et al., Journal of Nuclear Materials **363-365** (2007) 555-559
[6]. J.P. Gunn et al, proc. 22nd IAEA Fusion Energy Conference, Geneva 2008, EX/P6-32
[7]. A. Kaye, T. Brown, V. Bhatnagar, P. Crawley, et al., Fusion Enginering and Design **24**, 1 (1994)
[8]. D. Borodin, A. Kirshner et al., Physica Scripta **T128** (2007) 127–132
[9]. A. Czarnecka, et al., Proc. 37th EPS Conf. on Plasma Physics , Dublin, Ireland, 21-25 June 2010, ECA 34 (2010) P5.147; also to appear in Plasma Phys. Control. Fusion (Special issue: JET Task Force H 2011)
[10]. L. Colas et al., Nuclear Fusion **45** (2005) 767–782

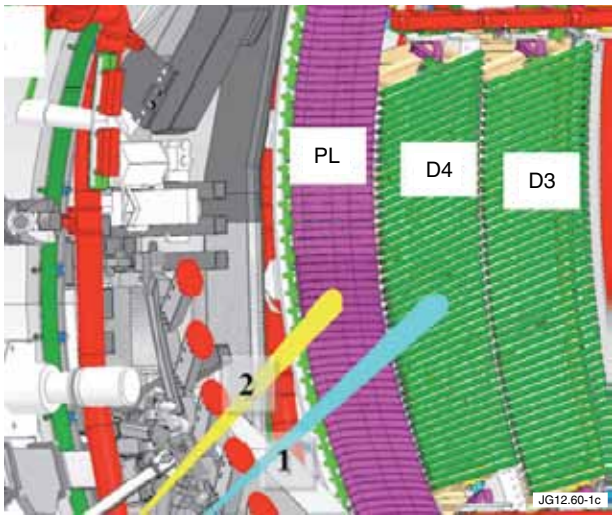

Figure 1: Illustration of the optical spectroscopy sightlines used to measure Be line emission at and near JET ICRH antenna D, with sightline 1 terminating near the center of Strap D4 (passing near PL D-left on the antenna side) and sightline 2 terminating near the opposite facing side of PL D-left. Both of these are nearly on the equatorial plane.

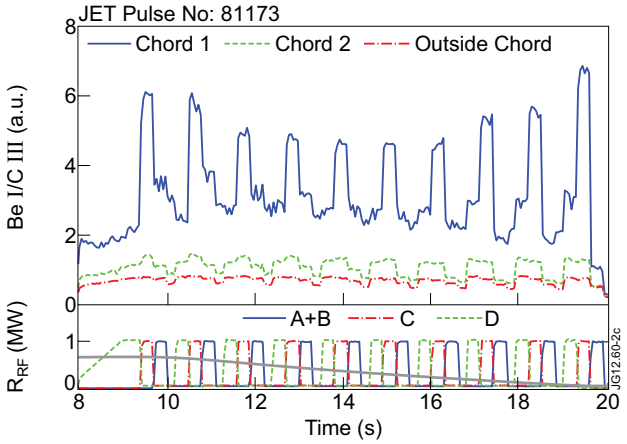

Figure 2: Be I emission, normalized to C III emission at the same location, for JET Pulse No: 81173 with sequential modulations of antennas C, D and A-B (2 straps of each A and B operated together as a single antenna) and simultaneous sweeping of the plasma current to vary the magnetic connections. In addition to the two antenna limiter viewing chords, a trace for an external (non-antenna) chord is also plotted. The powers of the antennas are plotted in the bottom graph window, together with a trace of the q_{95} variation with the plasma current sweep. Actual minimum and maximum values of the q_{95} at 3.0 and 4.2, respectively

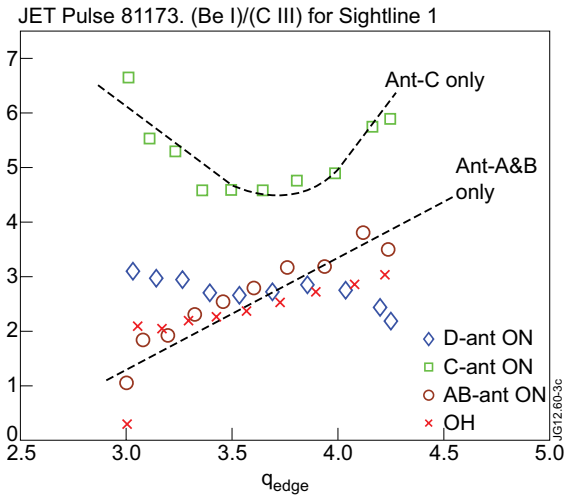

Figure 3. Values of Be I/C III, averaged over each antenna plateau and plotted against average value of q_{95} for each period of the sequential modulation of the antennas. Values given for all antennas, including the no-antenna (OH) plateaus, but only on the "D4-terminating" sightline, which shows the most significant variation during the q_{95} sweep in Fig.2. Although this chord terminates on the D4 strap, it passes by the D-left poloidal limiter and within 0.16 m from its antenna-facing side.

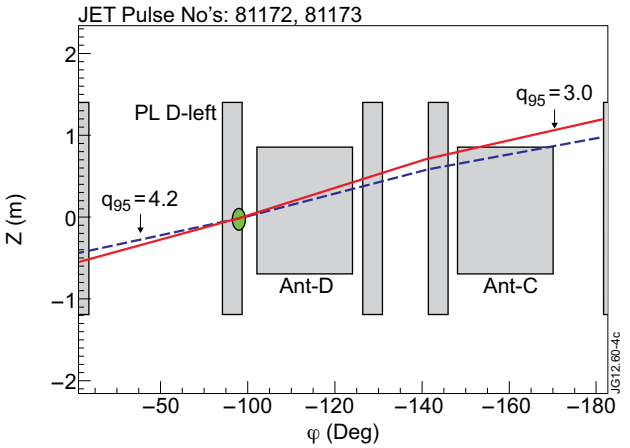

Figure 4. Magnetic fieldline tracing based on EFIT; the region of emission sampled by sightline '1' connects with regions at the top of antenna C, with the top corners corresponding to each of the maxima of Be I/C III in Fig.3. The abscisae and the ordinates are the toroidal and poloidal positions, respectively, in degrees.

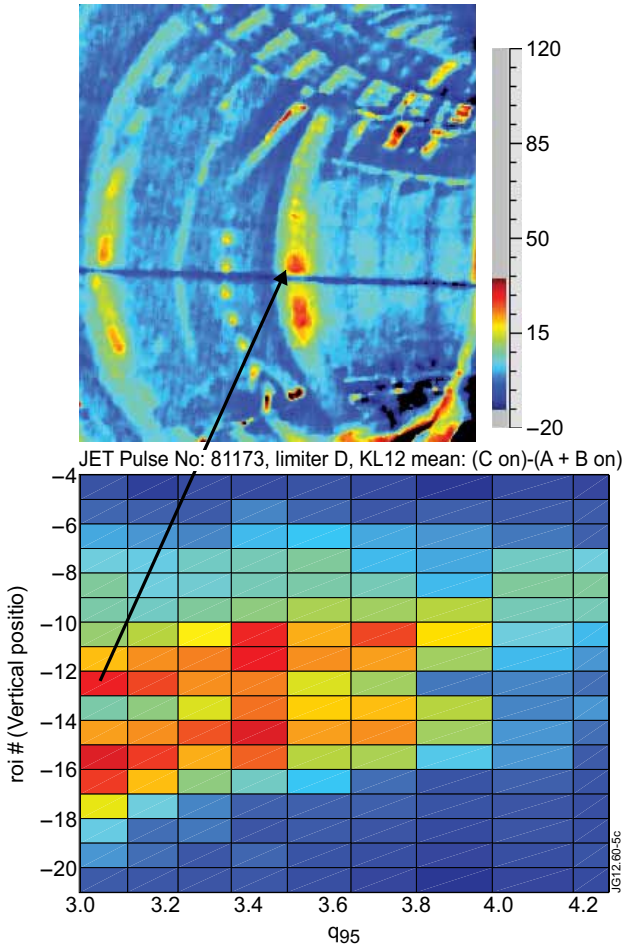

Figure 5: Top: image data from color camera viewing same poloidal limiter as the spectrometer sightlines and processing thereof: Top processed image results from RGB to luminance conversion and background subtraction. Bottom: the y axis represents the altitude index of Regions of Interest (ROIs) defined along the PL on the LHS of antenna D. The color represents the intensity of the camera signal averaged (spatially) in each ROI, when antenna C is energized. Signals were also averaged in time during each antenna-C sequence (~300ms). A&B equivalent signal at same q_{95} was treated.as backround and substracted.